Annual variations of T/ET in a semi-arid region: implications of plant water use strategies

Ruiqiang Yuan[1,2,3*], Liling Chang[3], Guoyue Niu[3]

[1] School of Environment and Resource, Shanxi University, Taiyuan, China

[2] Shanxi Laboratory for Yellow River, Taiyuan, China

[3] Department of Hydrology & Atmospheric Sciences, University of Arizona, Tucson, AZ, USA

* Corresponding author

Abstract

Understanding the annual variation in the transpiration to evapotranspiration ratio (*T/ET*) remains a challenge and is essential for a thorough understanding of plant responses to the changing environment. We obtained the annual dynamics of *T/ET* in a semi-arid area of the southwestern United States based on the medians of monthly *T/ET* derived from two *ET* partitioning methods. The variation in monthly *T/ET* was analysed, and plant water use strategies were discussed based on the water use efficiency evaluated by the transpiration (*WUE_T*). The results show that physiological changes in plants are vital in the annual dynamics of *T/ET*. Switches in plant physiological status (growth and dormancy) at the start and end of growing seasons induce two dramatic changes in *T/ET*. Consequently, there is an annual bimodal dynamic of monthly *T/ET*, with a maximum of 0.84 in October and a minimum of 0.14 in December. Physiological/biochemical variations of plants indicated by solar-induced chlorophyll fluorescence (*SIF*) are linearly related to *T/ET* in growing seasons at a monthly scale ($T/ET = 3.40 \times SIF + 0.36$, $R^2 = 0.987$). Generally, a stable high monthly *T/ET* occurs under sufficient energy and water conditions and a highly variable monthly *T/ET* occurs under energy and water deficient conditions. In semi-arid regions, plants can flexibly adjust *WUE_T*

following different water use strategies to survive or gain as much gross primary productivity (*GPP*) to compete. Saving water by greatly elevating *WUE_T* is the main strategy by which plants survive the non-growing season when *WUE_T* is linearly related to *SIF* (*WUE_T* = -114.93×*SIF* + 3.25, R^2=0.970). However, *GPP* and not *WUE_T*, becomes the goal of plants in growing seasons when they employ a stable and moderate *WUE_T* (around 2.1 gC kg^{-1} H_2O) despite the abundant energy and precipitation. There are obvious reductions in *WUE_T* during the transition periods of the plants' 'growth-dormancy' cycle. Our study highlights the importance of studying annual *T/ET* variations and water-use efficiency dynamics to better understand water use strategies in plants.

1. INTRODUCTION

Investigation of evapotranspiration (*ET*) partitioning in ecosystems can improve our understanding of the hydrological systems which affect the stream flow, groundwater recharge, and weather conditions, as well as the plant biomass production and associated carbon sequestration (Kool et al., 2014). The dynamics of transpiration (*T*) and the T/ET ratio are closely related to the vigour of terrestrial plants playing a crucial role in regulating atmospheric composition and climate (e.g., Suni et al., 2015). The water use efficiency evaluated based on the transpiration (*WUE_T = GPP/T*, *GPP* denotes the gross primary productivity), which describes the intrinsic trade-off between the carbon assimilation and water loss owing to the evaporation from stomas of leaves during CO_2 acquisition, is related to plant water use strategies. Studying the dynamics of *T* and *T/ET* is necessary for obtaining *WUE_T* variations and linking plant-water use strategies to environmental variability (Perez-Priego et al., 2018).

The dynamics of *T/ET* during growing seasons have been widely recognised. During growing

seasons, shrublands and grasslands in the southern United States display the lowest T/ET in the early growing season, owing to the time lag between precipitation pulses at the beginning of the rainy season, wetted root zone soil, and upregulated plants (Scott and Biederman, 2017). Globally, high *T/ET* has been observed in the late growing season of agricultural or natural ecosystems (Wang et al., 2014). *T/ET* and the leaf area index (*LAI*) increased during the growing seasons of grass, reflecting the surface controls of plants on *T/ET* (Wang et al., 2013). Recent results also indicate that *T/ET* may be less sensitive to the *LAI* than previously assumed, as a part of the covariation of *T/ET* and *LAI* could be attributed to other seasonal patterns such as the soil water availability or phenology cycles (Nelson et al., 2020). *LAI* and growing stage collectively explained 43% of the variation in *T/ET* (Wang et al., 2014). *LAI* has been shown to explain only small (20%) variations in the mean annual *T/ET* of agricultural or natural ecosystems (Li et al., 2019). No significant relationship was found between *T/ET* and *LAI* at diel, daily, or annual timescales for a temperate needle leaf forest (Berkelhammer et al., 2016). Fatichi and Pappas (2017) also found that *LAI* was not a key driver of the spatial variations of *T/ET*. In growing seasons, *T/ET* also changed with different precipitation patterns (with regard to the timing, frequency, duration, and intensity), which is considered as a part of water use strategies in a temperate deciduous forest (Gu et al., 2016). It has been reported that following a precipitation event of 9.7 mm, *T/ET* increased from 63.4 to 88.5% in a growing maize field as the upper soil layer dried out, while the plants accessed the deeper soil water (Hogan et al., 2020). In particular, water management can induce larger *T/ET* variations during the growing seasons in croplands compared to natural ecosystems (Xiao et al., 2018). However, considering the factors controlling the variations in *T/ET*, no clear correlation for annual precipitation, soil texture, or ecosystem type was found in drylands worldwide, and *T/ET* varied most during dynamic

wetting-drying episodes (Sun et al., 2019). Studies concerning *T/ET* in growing seasons have neglected the importance of seasonal *T/ET* variations to understand the factors controlling the *T/ET* variation and plant water use strategies. Recently, the annual dynamics of *T/ET* have been reported. In an annual cycle, variations in water availability strongly influenced not only the *T/ET* (Scott et al., 2021), but also the water use efficiency (*WUE_ET*, the water use efficiency evaluated based on *ET*) (Wang et al., 2021). The dynamics of *T/ET* may become complicated with varying levels of climatic and surface controls (precipitation, evaporative demand, water availability, leaf area, stomatal conductance, etc.). Despite these efforts, elucidating the annual *T/ET* dynamics and water use efficiency are still challenging, and the water use strategies incorporated in the annual dynamics of *T/ET* and water use efficiency have not been studied well.

Several *ET* partitioning methods have been developed to achieve reliable *T/ET* estimates (Kool et al., 2014). The stable isotope technique is a commonly used method, but is costly and laborious (Wang et al., 2010, 2013; Good et al., 2015). A typical uncertainty range for the stable isotope technique was ±21% (Xiao et al., 2018). The combined use of eddy covariance (EC) measurements and sap flow techniques provides a comprehensive method (Scott et al. 2006; Cammalleri et al., 2013). However, sap flow measurements are not representative of all species within the footprint of a flux tower. Scanlon and Kustas (2010) proposed a correlation analysis method based on the similarity theory. However, it requires high-frequency (10 Hz) turbulent data, which are not widely available, and tends to overestimate the soil flux components (*E*) (Klosterhalfen et al., 2019). Simple EC-based approaches are promising for future use in various ecosystems through the global flux tower networks. Zhou et al. (2014) proposed an underlying water-use efficiency ($uWUE = GPP \cdot VPD^{0.5}/ET$) model. Based on *uWUE*, *T/ET* can be estimated as the ratio of the apparent *uWUE*

(*uWUE*$_a$, estimated using the linear regression between *GPP*·*VPD*$^{0.5}$ and *ET*) over the potential *uWUE* (*uWUE*$_p$, estimated using the 95th quantile regression between *GPP*·*VPD*$^{0.5}$ and *ET*; Zhou et al., 2016). Scott's method for *T/ET* estimation is applicable when linear regressions between monthly *GPP* (abscissa) and monthly *ET* (ordinate) yield positive intercepts for months of the year. Subsequently, monthly *T/ET* is estimated based on the intercepts (considered as the multi-year average *E* for the month) along with the monthly *ET* (Scott and Biederman, 2017). However, the two EC-based methods are constrained by certain assumptions. The *uWUEp* is assumed to be relatively constant under steady-state conditions (e.g. relatively constant atmospheric CO_2 and water stress) for a given plant (Zhou et al., 2016 and Zhou et al., 2018). The assumption for Scott's method assumes that monthly *GPP* is a predictor of monthly *ET* based on the multi-year flux tower measurements (Scott and Biederman, 2017). Given the uncertainty or bias associated with a single partitioning method, using multiple methods to achieve reliable *T/ET* estimates is recommended (Hogan et al., 2020; Scott et al., 2021).

Based on the eddy covariance measurements in a semi-arid area, we estimated the monthly *T/ET* ratios using EC-based approaches proposed by Zhou et al. (2016) and Scott et al. (2017) for the growing and non-growing seasons from 2008 to 2015. The major purpose of this study was to reveal the annual variation patterns of *T/ET* and *T* in semi-arid regions. The secondary objective was to reveal plant water use strategies for their survival in a changing environment.

2. DATA and METHODS

2.1. Sites and data

The study area was Santa Rita, southeast Arizona, USA. Santa Rita is a semi-arid land located

between the Chihuahua and Sonoran deserts. The land cover comprises mainly desert shrublands, grasslands, and savanna lands. The Köppen climate type is ‘Bsk’, a steppe with warm winters. The long-term mean annual temperature is 17 °C. The annual mean precipitation is approximately 320 mm, with an annual potential *ET* of 1400 mm. The rainy season spans from July to September. The growing season spans from March to October. The non-growing seasons span from December to February, namely the winter months.

We obtained the EC and meteorological data from two AmeriFlux sites in Santa Rita (US-SRG, grassland with tree and shrub cover, whose data are available from 2008 to 2015; and US-SRM, woody savanna lands with grassland and shrub cover, whose data are available from 2008 to 2015). Vegetation fluorescence is the light emitted from chlorophyll during photosynthesis (Parazoo et al., 2014). Solar-induced chlorophyll fluorescence (*SIF*), measured by satellites, is sensitive to both structural and biochemical variations in vegetation (Yang et al., 2015; Sun et al., 2017; Smith et al., 2018). We used a 0.05° GOSIF product (Li and Xiao, 2019) to indicate variations in the vegetation of Santa Rita. The land cover of Santa Rita and the *SIF* pixels of the two sites were desert shrubs, grasses, and trees (Figure 1). The proportions of grasses, shrubs, and trees were different between the two sites. Despite this difference, the land cover of the two sites is typical to Santa Rita. A pooled dataset of the flux data from the two sites and the *SIF* data of the two pixels approximately represents the dynamics of climate and vegetation in Santa Rita.

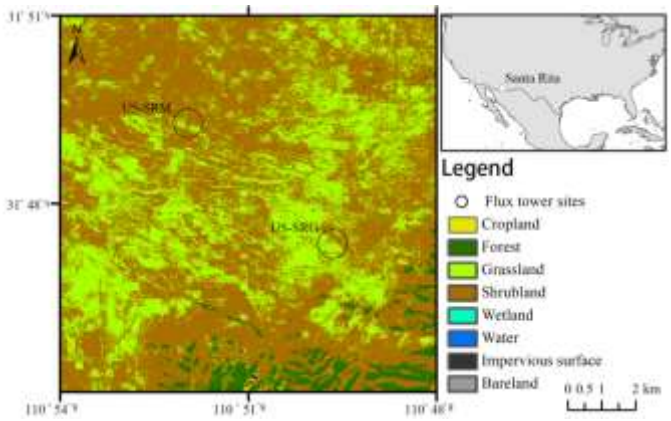

FIGURE 1 Land use and land cover in Santa Rita (land use and land cover data was downloaded from http://data.ess.tsinghua.edu.cn/fromglc10_2017v01.html in January 2021).

2.2. Methodology

Based on the half-hourly observations at the two sites, we calculated the *GPP* using the R package 'REddyProc' (Wutzler et al., 2018) and estimated the *ET* from latent heat. A standard and extensible EC data post-processing was executed by the package, including uStar-filtering (Papale et al., 2006), gap-filling (Reichstein et al., 2005), and flux-partitioning (Lasslop et al., 2010). We pooled the meteorological observations, flux data, and *SIF* data of the two sites to gain medians of those variables for the months of a year, to obtain representative annual dynamics of the variables in Santa Rita.

We calculated the monthly *T/ET* for the two sites using Scott's and Zhou's methods, respectively. We calculated the monthly *T/ET* using Zhou's method in three stages of a year: March – June (the pre-monsoon phase with high energy and low water availability), July – September (the monsoon phase with high energy and high water availability), and October – February (the period with low energy and low water availability), respectively. We calculated the monthly *T/ET* ratios using Scott's method when the linear correlation between the monthly *GPP* and *ET* was sufficiently high

(Pearson's $r \geq 0.7$). The results of the two ET partitioning methods were compared, and the Pearson's *r* of linear regressions between the results was calculated by months of a year. Subsequently, the result of Zhou's method was corrected (the *T/ET* estimates of Zhou's method as a predictor of the results of Scott's method) to reduce the uncertainty, which is explained in section 3.2. Although both Scott's and Zhou's methods have uncertainty, the corrected *T/ET* estimates enhance the common variance of *T/ET* contained in the two results. We grouped the months within a year (stages as mentioned above) during the correction to ensure that the Pearson's *r* of linear regressions between the results is higher than 0.7. The *T/ET* from Zhou's method in January, February, and December was directly employed, as explained in section 3.2. Based on the corrected monthly *T/ET*, the monthly transpiration ($T = ET \cdot T/ET$) and leaf scale water use efficiency were calculated. Finally, the corrected monthly *T/ET*, calculated monthly *T*, and *WUE_T* were obtained, and their medians were calculated for months of the year to represent the responses of mixed vegetation in Santa Rita to the changing environment.

3. RESULTS

3.1. Annual patterns of climate and surface controls

The annual patterns of net radiation (*Rn*), precipitation (*P*), relative humidity (*RH*), *GPP*, *ET*, and *SIF* are shown in Figure 2. *Rn* consistently increases until May, reaches a plateau from May to August, and gradually decreases thereafter. Approximately 74% of the precipitation occurs during rainy seasons, which is associated with the North American monsoon system (Perez-Ruiz et al., 2010). Plants gain sufficient energy and water during the rainy season. In May and June, precipitation is almost at its lowest level with an *RH* below 20%, while *Rn* is close to its peak value

when the study area is in its driest state; namely, the pre-monsoon drought (Figure 2). The study area is in its wettest state during July and August when the soil moisture content could recover, accompanied by a humid atmosphere (*RH* around 50%) due to abundant rainfall in rainy seasons. In winter, there are obvious energy and water deficiencies. However, *the RH* was relatively high.

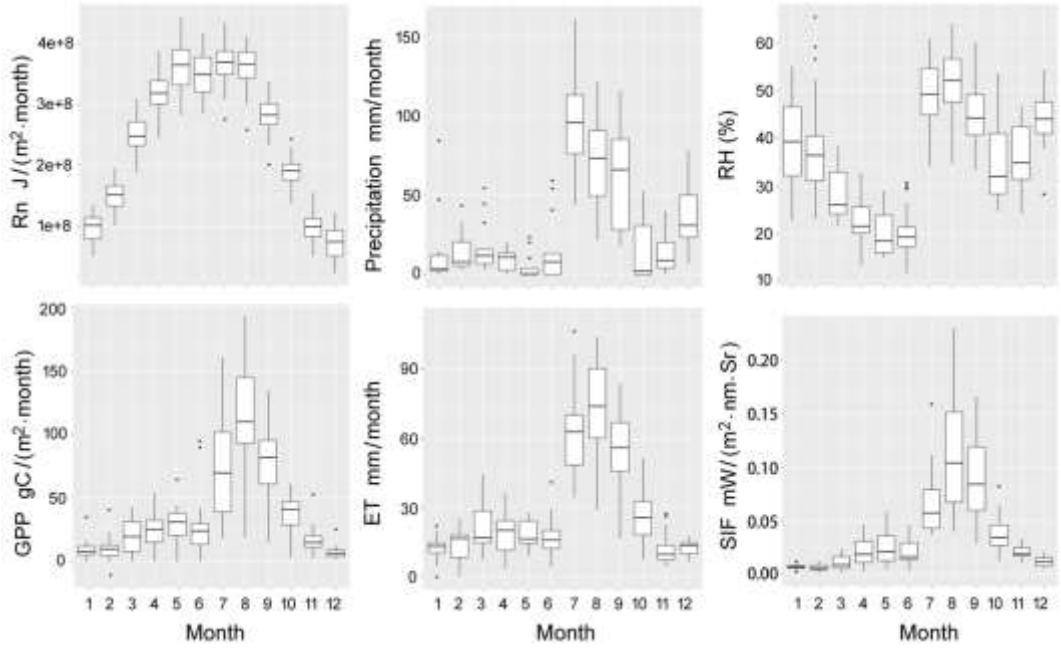

FIGURE 2 Box plots of monthly *Rn*, precipitation, *RH*, *GPP*, *ET*, and *SIF* in Santa Rita. The meteorological measurements and flux data are from the two AmeriFlux sites (US-SRM and US-SRG) from 2008 to 2015. The SIF data of Santa Rita is from the GOSIF product for the same period. The statistic features of the variables for the months of a year indicate the seasonal variation of the climatic controls and surface controls in Santa Rita.

GPP, *ET*, and *SIF* are stimulated by sufficient precipitation and are constrained by insufficient *Rn*. Consequently, they are in the high-level stage during the main growing seasons (from July to October), and in the low-level stage during the pre-monsoon growing seasons (from March to June) and non-growing seasons, displaying similar seasonal patterns. *GPP*, *ET*, and *SIF* are relatively low from March to June because of the pre-monsoon drought when the bare ground cover can increase

from approximately 45 to 60% (Scott et al., 2015).

3.2. ET partitioning results and annual dynamics of T/ET

The monthly *T/ET* result from Scott's method was unavailable for several months, including January, February, June, and December, due to the insufficient linear correlation (Pearson's $r < 0.7$) between monthly the *GPP* and *ET*. In the other months, the monthly *T/ET* estimates from Scott's method exhibited a clear linear correlation with those from Zhou's method (Figure 3), indicating that these two methods have grasped the common variations of the monthly *T/ET*.

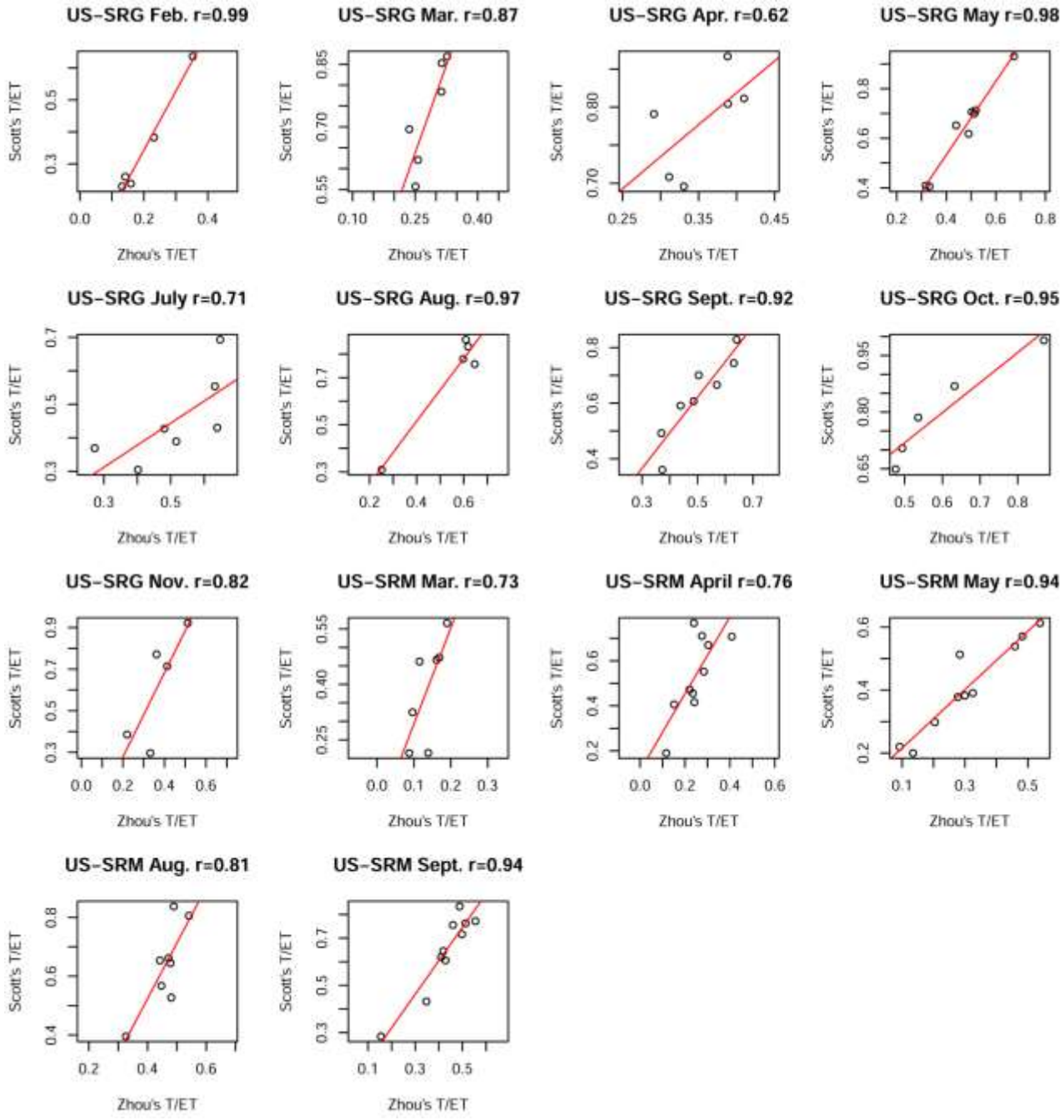

FIGURE 3 Correlation between the monthly T/ET ratios estimated by Zhou's and Scott's methods, respectively. The *r* represents the Pearson linear correlation coefficient. The red lines indicate the regression lines between Zhou's and Scott's T/ETs, respectively.

However, the results of Scott's method were greater than those of Zhou's method (Figure 3). Given that Scott's method was verified by its comparison with direct measurements at Santa Rita (Scott and Biederman, 2017), Zhou's method might underestimate *T/ET*. This is possibly the case in

dry land. First, *uWUEp* is generally higher under water stress conditions than under non-stress conditions. Second, a higher quantile in the quantile regression of Zhou's method produces a greater estimation of *uWUEp* and, consequently, an underestimation of *T/ET*. As shown in Figure 4, the monthly mean *T/ET* increases by 22% on average when a 90% quantile is used to calculate the *uWUEp*, compared to that using the 95% quantile. Our results show less influence of different quantiles on the *T/ET* estimation in December, January, and February (Figure 4), indicating the robustness of the estimation during periods with low *T/ET*. Therefore, we corrected the results of Zhou's method according to those of Scott's method to achieve *T/ET* estimates and enhance the common variations contained in the two results, with no corrections for December, January, and February.

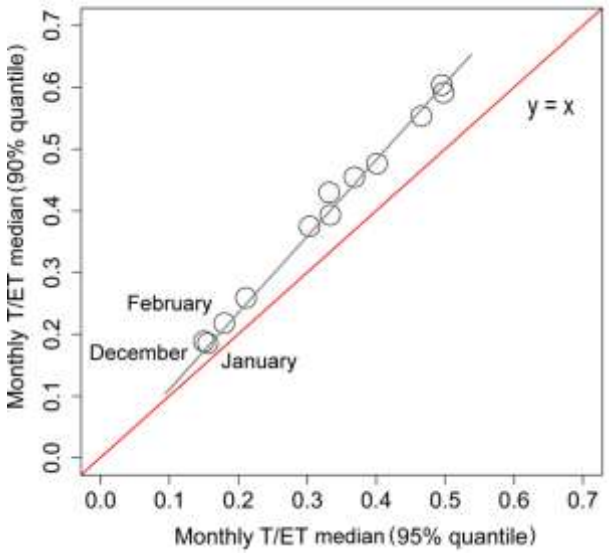

FIGURE 4 Comparison of results with different quantiles in Zhou's method. Monthly *T/ET* medians derived by a 90% quantile are 22% higher than those by a 95% quantile on average. High quantiles contribute to the underestimation of *T/ET*. As indicated by the regression line, the underestimation increases with an increase in the *T/ET* ratio. The points of January, February, and December are closer to the 1:1 line than other months, suggesting that the estimation of *T/ET* in these months are

relatively insensitive to different quantiles.

We combined the corrected monthly *T/ET* with the *T/ET* estimates from Zhou's method in January, February, and December to represent the *T/ET* estimates in the months of a year (Figure 5). Scott and Biederman reported that the monthly T/ET of the two sites change from 0.45 – 0.54 in July, 0.62 – 0.69 in August, and 0.54 – 0.66 in September, respectively (Scott and Biederman, 2017). These results fall within the scope of our results (average ±1 standard deviation). Although it is almost impossible to conduct an absolute validation for the partitioning results, it is interesting to achieve an annual dynamic of monthly *T/ET* based on the medians of monthly *T/ET* estimates. According to our estimates, the monthly *T/ET* median reached its maximum (0.84) in October and dropped to its lowest level (0.14) in December. The monthly *T/ET* ratios were low in non-growing seasons with monthly *T/ET* medians not more than 0.21. Furthermore, there are two sharp changes in the annual dynamics of the monthly *T/ET*. The first significant change occurs in March when *T/ET* sharply rises from 0.16 to 0.56. The second occurs in December, with a quick drop of *T/ET* from 0.82 to 0.14.

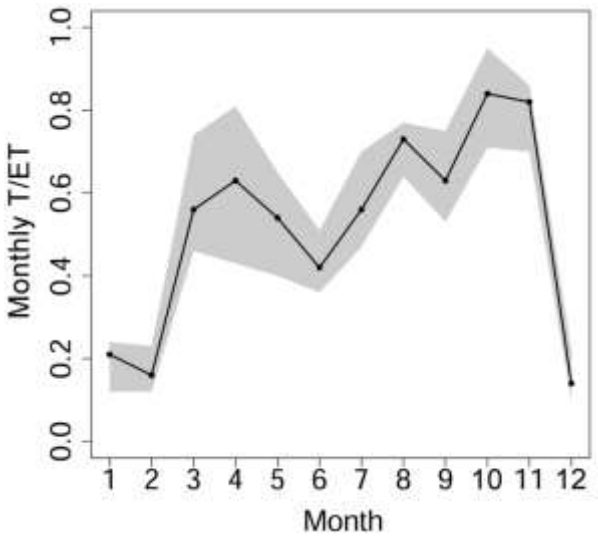

FIGURE 5 Annual dynamic of the monthly *T/ET*. Monthly *T/ET* medians are indicated by black dots. The grey shadow indicates the range from 25 to 75% quantiles of monthly *T/ET*.

3.3. Annual change of transpiration and leaf scale water use efficiency

Monthly *T* was calculated as the product of the monthly *T/ET* estimates and *ET*. The largest *T* was 91 mm month^{-1} during the observation period in Santa Rita, while the lowest was only 0.7 mm month^{-1}. *T*, as an indicator of physiological/biochemical variations in vegetation, is constrained by the energy input and water availability. Our results showed that vegetation consumes more water (average *T* of 37 ± 19 mm month^{-1}) during the main growing season when the energy and water inputs were abundant (Figure 6). In the pre-monsoon growing seasons, the energy input is moderate, while precipitation is scarce; thus, *T* is obviously lower (average *T* of 12 ± 8 mm month^{-1}) than that in the main growing season. In the non-growing season (winter), *T* is generally not more than 8.5 mm month^{-1} with an average of 3 ± 2 mm month^{-1}.

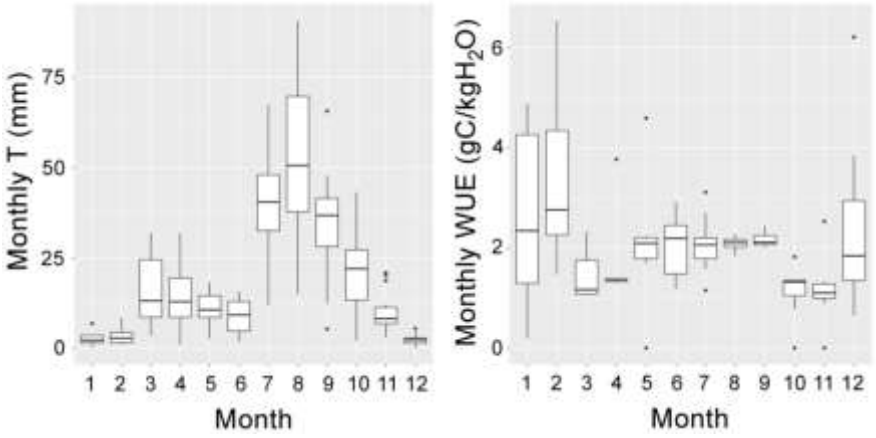

FIGURE 6 Monthly transpiration and *WUE_T* in Santa Rita.

The monthly *WUE_T* ranges from 0 to 6.54 gC kg^{-1} H_2O (Figure 6). Medians of *WUE_T* for months of a year change between 1.1 and 2.8 gC kg^{-1} H_2O, which is comparable to the range from 0.8 to 2.4 gC kg^{-1} H_2O across dryland ecosystems in an arid region in Northwest China (Wang et al., 2021). The monthly *WUE_T* varies greatly in January, February, March, June, and December, when the growth is obviously hindered by insufficient energy and/or water stress which would significantly

change ecosystem functions (Gu et al., 2016). Simultaneously, the monthly *WUE_T* is less variable in the other months than in these five months. According to the monthly *WUE_T* medians, months of a year can be divided into two groups by the value 1.6 gC kg^{-1} H_2O. The low monthly *WUE_T* group includes March, April, October, and November which denote the start and end of the growing seasons or the transition periods between non-growing and growing seasons. The high monthly *WUE_T* group included the other months of the growing and non-growing seasons. It is obvious that the *WUE_T* of plants is different between winter and summer in the semi-arid area. However, it has been reported that *WUE_ET* does not differ between winter and summer (Biederman et al., 2018). Notably, *WUE_T* and *WUE_ET* (*GPP*/*ET*) might result in opposite results.

The annual *WUE_T* dynamic does not follow the pattern of energy (*Rn*), water availability (*P*), or physiological/biochemical activities (*SIF*), and is thus distinct from *T*. The amount of water that can be used by plants (i.e. *T*) can be determined by *Rn*, *P*, and *SIF*; but how this water is used (namely *WUE_T*) is influenced by the plant water use strategies. The water use strategies of plants in a changing environment thus provide a deeper understanding of plant adaptability.

4. DISCUSSION

4.1. Variations of T/ET in an annual cycle

Reliable estimates of monthly *T/ET* produced reasonable estimates of the monthly *T*. There is often a strong relationship between the *ET* and *GPP* at water-limited sites (Law et al., 2002). In our case, the linear correlation coefficient between the monthly *GPP* and *ET* was 0.92 (Pearson's *r*). Stomatal conductance critically determines both the photosynthetic uptake of CO_2 and the loss of water transported from the leaf (Zhou et al., 2014). Thus, a better linear correlation between monthly

GPP and *T* was achieved (r = 0.96), suggesting the reliability of *T* and consequently, the *T/ET* estimates.

The monthly *T/ET* estimates for the main growing seasons are reasonable. During the main growing seasons, the *T/ET* ratio was 0.58 for the Chihuahuan Desert shrubland (Scott et al., 2006). Schlesinger and Jasechko (2014) found similar *T/ET* ratios of 0.54 ± 0.18 and 0.57 ± 0.19 for temperate grasslands, respectively. The *T/ET* of desert shrubs in northern China was 0.64 during the growing seasons, with groundwater being the main water source for plant transpiration and soil evaporation (Zhao et al., 2016). Rain-fed spring maize transpiration accounted for 59 and 56% of *ET* in the semi-arid Loess Plateau of China (Gao et al., 2018). In the semi-arid Santa Rita, the monthly *T/ET* of the main growing season is 0.68 ± 0.19 for the vegetation, which is consistent with previous estimates ranging from 0.55 to 0.75 for southeast Arizona (Hamerlynck et al., 2014). Furthermore, the monthly *T/ET* median reached a peak in October (0.84) in our case. Similarly, the *T/ET* ratio approached 0.91 at the end of the growing season in a cold semi-arid site in China, wherein grassland and woodland were the dominant land cover types (Li et al., 2016). In October, precipitation was greatly reduced as the rainy season passed, which could trigger a rapid drop in soil evaporation. However, moisture in the deep soil layer has a longer memory than precipitation (Stillman et al., 2014). The antecedent deep soil moisture supports plant *T* to generate a high *T/ET* in the post-monsoon period. We also confirmed that the time-lag induced the low *T/ET* in July. At the beginning of the rainy season, soil moisture gradually recovers, which activates the ecosystem activities (Cable et al., 2013; Biederman et al., 2018). However, precipitation must first satisfy the soil moisture deficit before being absorbed by the roots (Scott et al., 2017). It has been reported that vegetation *T* delays its responses to increased soil moisture for approximately three weeks after the

287 onset of the monsoon (Cavanaugh et al., 2011).

288 The monthly *T/ET* medians change between 0.42 and 0.63 in the pre-monsoon growing seasons
289 and between 0.56 and 0.73 in the main growing seasons, respectively. In the pre-monsoon growing
290 seasons, plants are suppressed by the pre-monsoon drought, as revealed by the low *P*, *SIF*, *T*, and
291 *GPP*, which induces lower *T/ET* values than those in the main growing seasons.

292 Changes in the physiological status of plants related to dormancy contribute to two dramatic
293 changes in the monthly *T/ET* before and after non-growing seasons. The lowest energy input in an
294 annual cycle and limited precipitation forces plants into dormancy (Perez-Ruiz et al., 2010). We
295 confirmed that plants with inactive physiological/biochemical activities become dormant in the
296 winter months, as indicated by the drops in *SIF, GPP,* and *T* to their annual minimums. The very low
297 *T/ET* ratios in non-growing seasons are appropriate for dormant plants. Additionally, plant mortality
298 coinciding with disadvantageous conditions (Hamerlynck et al., 2013) could further limit the *T/ET*
299 ratios. After the non-growing seasons, the energy input (*Rn*) sharply increased by 75% in March,
300 which is the largest annual change in monthly *Rn*. Simultaneously, the precipitation is approximately
301 the sum of the previous two months. The disadvantageous conditions disappeared, and plants were
302 subsequently upregulated out of dormancy, which can be verified by the significant increases in *SIF*,
303 *T,* and *GPP* in March. The re-upregulated plants produced a large increase in *T/ET* from February to
304 March. Before the non-growing seasons, plants were suppressed by persisting decreases in energy
305 input and limited precipitation, with a 63 and 64% decrease in *T* and *GPP* in November compared to
306 October, respectively. However, the *SIF* only declined by 45%. Compared to *T* (*GPP*), which is
307 controlled by stomata, the relatively weak *SIF* response indicates that plants struggle to maintain
308 physiological/biochemical activities before falling into dormancy. A fairly high monthly *T/ET*

median is produced by struggling plants. However, plants eventually downregulate and resume dormancy by suppressing the climate control (*Rn*, *P*, and *RH*). Consequently, *T/ET* quickly dropped by 83% in December, relative to November.

As shown in Figure 7, there is a strong linear relationship between the monthly *SIF* and *T/ET* from June to September ($T/ET = 3.40 \times SIF + 0.36$, $R^2 = 0.987$). *SIF* is directly related to the structural, physiological, and biochemical variations in vegetation (Yang et al., 2015; Sun et al., 2017; Smith et al., 2018). Therefore, *SIF* is a good plant metric for *T/ET* dynamics. According to our results, plants can have a dominant influence on the *ET* partitioning during the growing seasons in a semi-arid area.

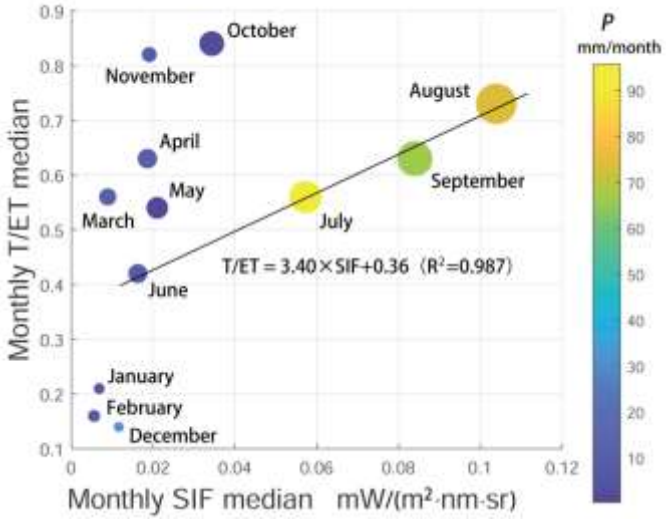

Figure 7 A **s**catter plot of *SIF* and *T/ET*. The colour of dots indicates the magnitude of monthly precipitation. The size of dots indicates the magnitude of monthly *GPP*.

However, we could not find a single driving factor solely responsible for the intra-annual dynamics of *T/ET* (Figure 7). The seasonal course of *T/ET* is related to both surface and climatic controls (Scott et al., 2017). In our case, the annual dynamics of *T/ET* are closely related to *Rn*, *P*, *SIF*, *T*, and *GPP*, suggesting the climatic and physiological controls on *ET* partitioning. Climatic controls tend to produce a *T/ET* pattern similar to those of *SIF*, *T*, and *GPP* in the semi-arid area,

while physiologic controls of plants probably break the pattern. Therefore, in an annual cycle, the *T/ET* ratio does not depend on any single factor. For example, the climate might be similar between February and November, but the physiological status related to dormancy differs. Hence, the monthly *T/ET* medians were obviously different between the two months. We summarized the annual dynamics of monthly *T/ET* as follows. When active plants are met with sufficient energy and water, the monthly *T/ET* will be high and the mean anomaly will be low, suggesting a stable high monthly *T/ET*. For example, in July, August, and September (Domain 1 in Figure 8), the monthly *T/ET* mean is 0.64 and the mean anomaly is only 0.06. When suppressed plants are subjected to energy and water deficiencies, the mean anomaly of monthly *T/ET* is high, suggesting that it is highly variable. For example, the mean anomaly of monthly *T/ET* from October to February is 0.33 (Domain 3 Figure 8).

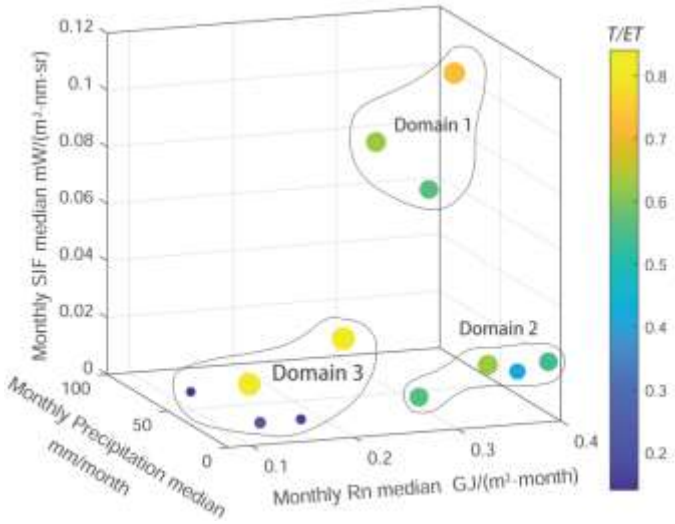

FIGURE 8 Variation of monthly *T/ET* median along with the *Rn*, *P*, and *SIF*. The color and size of dots indicate the magnitude of T/ET. The energy and water are sufficient for plants to grow in Domain 1, where differences of T/ET are small. In Domain 3, where the T/ET differs greatly, small SIF values with low energy and water inputs represent a disadvantageous stage. The energy input is high, but the water input is low in Domain 2, where the differences of T/ET are moderate.

4.2. Plant water use strategies

WUE_ET variability in arid ecosystems is primarily controlled by physical processes in semi-arid and sub-humid regions (Yang et al., 2016). In our case, *WUE_T* might be regulated not only by physical processes (water stress and heat stress), but also by biological processes (transpiration, dormancy, germination, senescence, water, and nutrient storage). Plants respond to regulations that reveal a wide range of water use strategies.

Plants employ a moderate *WUE_T* during growing seasons to obtain as much *GPP* in semi-arid areas. Notably, plants seem to 'waste' water by employing a moderate *WUE_T* in growing seasons (Figure 9). In particular, precipitation can affect leaf-level physiology through the direct dilution of soil nitrogen (Patrick, et al. 2009). Dilution could be obvious in the semi-arid area due to abundant monsoon precipitation. Consequently, excess *T* is needed for plants to procure sufficient nutrients to obtain as much *GPP* as possible in the main growing seasons. Moreover, *WUE_T* begins to decline when the leaf is exposed to temperatures exceeding the optimum (Hatfield and Dold, 2019). Therefore, overshoots in the stomatal opening are common features of plants under heat stress, resulting in water loss to maintain the leaf temperature and maximize the *GPP* production (Lawson and Vialet-Chabrand, 2019). With sufficient energy and water, *GPP* production and not water use efficiency, has become the main concern for plants.

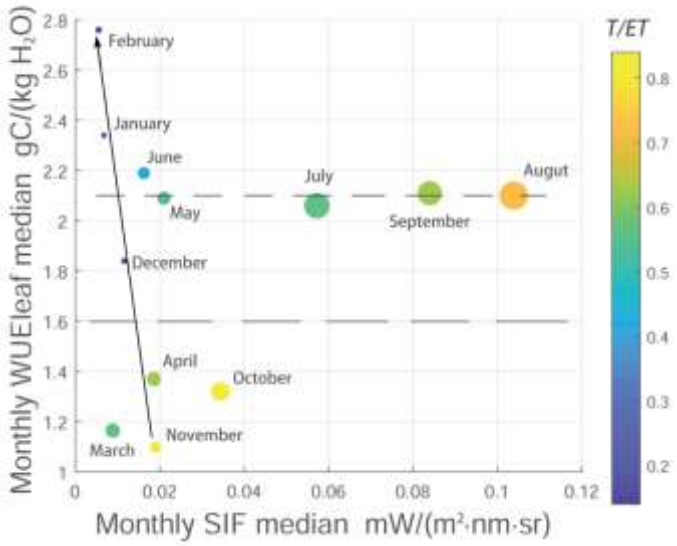

Figure 9 Monthly *SIF* medians versus monthly *WUE_T* medians. The size of the dots is directly proportional to the magnitude of monthly transpiration medians. The upper and lower dashed lines indicate 2.1 gC kg^{-1} H_2O (the average from May to September) and 1.6 gC kg^{-1} H_2O (dividing the two groups), respectively.

Plants employ an almost constant monthly *WUE_T* during the growing season. Zhou et al. (2014) demonstrated that the underlying water use efficiency (describing a linear relationship between $A\sqrt{GPP}$ and T; A is the rate of CO_2 assimilation) at the leaf scale remains essentially constant for certain vegetation types during the growing season. In our case, the monthly *WUE_T* median remained almost unchanged (with an average of 2.1 gC kg^{-1} H_2O) from May to September, despite the large variations in the monthly *SIF* (Figure 9), which is obviously different from the increase in the monthly *T/ET* median (Figure 7). More efforts are required to explain the almost constant monthly *WUE_T* during the growing seasons. It has been reported that water use efficiency increases under water-stress conditions (Tong et al., 2019), reflecting the adaptability of plants in semi-arid areas to water deficiency (Wang et al., 2021). Stomata are key players in the response of plants to water stress (Gambetta et al., 2020). The reduction in photosynthesis is less than that in

stomatal conductance, which explains the increase in water use efficiency under water-deficit stress conditions (Hatfield and Dold, 2019). In our case, the monthly *WUE_T* median in June was slightly higher than that in other months as a result of the water stress at the end of the pre-monsoon drought. Both *GPP* and *SIF* decreased by 23% in June compared to May, indicating a reduction in photosynthesis. Although we did not measure the stomatal conductance, a very dry condition can be confirmed based on limited precipitation and considerably low *RH* in June, which suggests reduced stomatal conductance (Grossiord et al., 2020).

Plants survive the non-growing seasons by greatly enhancing *WUE_T*. Plants (here evergreen shrubs) have to continue *GPP* production to survive the non-growing seasons. However, *T* in non-growing seasons is less than 3 mm $month^{-1}$ on average and is less variable than that of the growing seasons. To deal with this, plants conduct highly efficient *GPP* production. According to our result, the monthly *WUE_T* median greatly increased from 1.10 gC kg^{-1} H_2O (November) to 2.76 gC kg^{-1} H_2O (February), with an increment of around 0.42 gC kg^{-1} H_2O per month (Figure 9). Finally, plants increase the monthly *WUE_T* by up to 130.8% of the average *WUE_T* in growing seasons, possibly due to the disappearance of heat stress. The process can be described as $WUE\_T = -114.93 \times SIF + 3.25$ (R^2=0.970), suggesting a high sensitivity of *WUE_T* to *SIF* in non-growing seasons. The rapid increase in *WUE_T* suggests a strong adaptability of plants to the changing environment in semi-arid Santa Rita. Rapid stomatal responses have been reported to greatly improve the water-use efficiency (McAusland et al., 2016). To a certain degree, the strong adaptability could be supported by the rapidity of stomatal responses in the stomatal pore apertures, size, and density in changing environments (Bertolino et al., 2019).

Plants employ a low *WUE_T* during the transition of the ‘growth-dormancy’ physiological cycle,

possibly to prepare for the subsequent stage. According to our results, *WUE_T* changed between 1.1 and 1.4 gC kg^{-1} H_2O in the transition periods, which was significantly lower than that in the growing and non-growing seasons (Figure 9). The decrease in *WUE_T* in March and April is possibly related to the germination during plant physiological/biochemical upregulation. The decline of *WUE_T* in October and November might be a result of the grass senescence and water storage in shrubs and tree bodies during low production periods. Further studies are required to explain the decline in *WUE_T* during the transition of the 'growth-dormancy' physiological cycle.

5. CONCLUSIONS

In an annual cycle, the average monthly *T/ET* medians of vegetation composed of grasses, shrubs, and savanna is 0.52±0.24 in the semi-arid Santa Rita, Arizona (southwestern USA), with a maximum of 0.84 in October and a minimum of 0.14 in December. There is a bimodal annual dynamic of monthly *T/ET* medians. The monthly *T/ET* medians change from 0.42 to 0.63 in the pre-monsoon growing season (March-June) and from 0.56 to 0.84 (July-October) in the main growing season. The monthly *T/ET* median is at a minimum in June during the growing seasons under the water stress of the pre-monsoon drought. In the non-growing season (from December to February), the monthly *T/ET* medians are not more than 0.21, forming the other valley. We found a strong linear relationship between *SIF* and *T/ET* from June to September ($T/ET = 3.40 \times SIF + 0.36$, $R^2=0.987$). *SIF* is a good plant metric for *T/ET* dynamics.

Climate controls, especially the energy input, stimulate plants' physiological status, which is crucial in the annual *T/ET* dynamics. Changes in the plant physiological status related to the dormancy contribute to the two dramatic changes in monthly *T/ET.* When the energy input increases

418 greatly in spring, plants can quickly revert from dormancy, producing a dramatic increase in *T/ET*.
419 When the energy input decreases greatly after growing seasons, plants dramatically decrease the
420 biomass production but produce the highest monthly *T/ET*. A dramatic decrease in *T/ET* occurred
421 when plants became dormant. Consequently, plants can have a dominant influence on the *ET*
422 partitioning in semi-arid areas.

423 In semi-arid regions, plants implement different water use strategies to adapt to changing
424 environments. The monthly *WUE_T* median remained almost unchanged (2.1 gC kg^{-1} H_2O on
425 average) from May to September in growing seasons, despite the large variations in monthly *SIF*.
426 However, the monthly *WUE_T* median greatly increased from 1.10 to 2.76 gC kg^{-1} H_2O from
427 November to February in non-growing seasons, displaying a high sensitivity to *SIF* (*WUE_T* =
428 -114.93×*SIF* + 3.25, R^2=0.970). Highly efficient production under conditions that inhibit
429 transpiration (less than 3 mm $month^{-1}$) is the core strategy for plant survival in non-growing seasons.
430 However, with abundant energy and precipitation, plants employ only a moderate *WUE_T* in the
431 growing seasons. On the one hand, focusing on production (and not the water use efficiency)
432 becomes the key strategy for plants with sufficient energy and water. Conversely, the moderate
433 *WUE_T* is considered to be a result of heat stress. Additionally, low *WUE_T* values were employed
434 at the start and end of the growing season, which is considered as the transition during the
435 'growth-dormancy' physiological cycle of plants. The reduction of *WUE_T* during the transition is
436 believed to be a water use strategy for plants to prepare for upregulation/downregulation out of or
437 into dormancy. Further studies are required to address the global variation in *T/ET* dynamics,
438 *WUE_T*, and related water use strategies.

ACKNOWLEDGEMENTS

This research project was funded by the NASA MAP Program (80NSSC17K0352), NOAA OAR's OWAQ (NA18OAR4590397), and the China scholarship council (201708140009). We thank the anonymous reviewers for their valuable comments on our draft paper. We thank Dr. Russell L. Scott for his support with flux tower data processing. We thank Dr. Sha Zhou for her support with the quantile regression in R.

REFERENCES

Berkelhammer, M., Noone, D. C., Wong, T. E., Burns, S. P., Knowles, J. F., Kaushik, A., et al., 2016. Convergent approaches to determine an ecosystem's transpiration fraction: Transpiration fraction of two forests. Global Biogeochemical Cycles, 30(6), 933–951. https://doi.org/10.1002/2016G B005392

Bertolino, L.T., Caine, R.S., Gray, J.E., 2019. Impact of Stomatal Density and Morphology on Water-Use Efficiency in a Changing World. Front Plant Sci, 10: 225. DOI:10.3389/fpls.2019.00225

Biederman J., Scott R., Arnone I., John A., Jasoni R., Litvak M., Moreo M., Papuga S., Ponce-Campos G., Schreiner-McGraw A., Vivoni E., 2018. Shrubland carbon sink depends upon winter water availability in the warm deserts of North America. Agricultural and Forest Meteorology, 249, 407–419.

Cable, J. M., Ogle, K., Barron-Gafford, G. A., Bentley, L. P., Cable, W. L., Scott, R. L., Williams, D. G., Huxman, T. E., 2013. Antecedent Conditions Influence Soil Respiration Differences in Shrub and Grass Patches. Ecosystems, 16, 1230–1247.

Cammalleri, C., Anderson, M.C., Gao, F., Hain, C.R., Kustas, W.P., 2013. A data fusion approach for mapping daily evapotranspiration at field scale. Water Resources Research, 49(8): 4672-4686. DOI:https://doi.org/10.1002/wrcr.20349

Cavanaugh, M. L., Kurc, S. A., Scott, R. L., 2011. Evapotranspiration partitioning in semiarid shrubland ecosystems: a two-site evaluation of soil moisture control on transpiration. Ecohydrology, 4, 671–681.

Fatichi, S., Pappas, C., 2017. Constrained variability of modeled T:ET ratio across biomes: Transpiration: Evapotranspiration Ratio. Geophysical Research Letters, 44(13), 6795–6803.

Gambetta, G.A. et al., 2020. The physiology of drought stress in grapevine: towards an integrative definition of drought tolerance. Journal of Experimental Botany, 71(16): 4658-4676. DOI:10.1093/jxb/eraa245

Gao, X. et al., 2018. Evapotranspiration partitioning and energy budget in a rainfed spring maize field on the Loess Plateau, China. CATENA, 166, 249-259.

Good, S. P., Noone, D., Bowen, G., 2015. Hydrologic connectivity constrains partitioning of global terrestrial water fluxes. Science, 349, 175–177.

Grossiord, C. et al., 2020. Plant responses to rising vapor pressure deficit. New Phytologist, 226(6): 1550-1566. DOI:10.1111/nph.16485

Gu, L., Pallardy, S. G., Hosman, K. P., Sun, Y., 2016. Impacts of precipitation variability on plant species and community water stress in a temperate deciduous forest in the central US.

Agricultural and Forest Meteorology, 217, 120–136.

Hamerlynck, P. E., Scott, R. L., Barron-Gafford, G. A., 2013. Consequences of Cool-Season Drought-Induced Plant Mortality to Chihuahuan Desert Grassland Ecosystem and Soil Respiration Dynamics. Ecosystems, 16, 1178–1191.

Hamerlynck, E. P., Scott, R. L., Cavanaugh, M. L., Barron-Gafford, G., 2014. Water use efficiency of annual-dominated and bunchgrass-dominated savanna intercanopy space. Ecohydrology, 7, 1208–1215.

Hatfield, J.L., Dold, C., 2019. Water-Use Efficiency: Advances and Challenges in a Changing Climate. Front Plant Sci, 10, 103. DOI:10.3389/fpls.2019.00103

Hogan, P. et al., 2020. High-Frequency Stable-Isotope Measurements of Evapotranspiration Partitioning in a Maize Field. Water, 12(11), 3048.

Li, Z., Qi, F., Wang, Q. J., Song, Y., Li, H., Li, Y., 2016. The influence from the shrinking cryosphere and strengthening evopotranspiration on hydrologic process in a cold basin, Qilian Mountains. Global and Planetary Change, 144, 119-128.

Li, X. and Xiao, J., 2019. A Global, 0.05-Degree Product of Solar-Induced Chlorophyll Fluorescence Derived from OCO-2, MODIS, and Reanalysis Data. Remote Sensing, 11(5), 517.

Klosterhalfen, A. et al., 2019. Source partitioning of H_2O and CO_2 fluxes based on high-frequency eddy covariance data: a comparison between study sites. Biogeosciences, 16(6), 1111-1132. DOI:10.5194/bg-16-1111-2019

Kool, D., Agam, N., Lazarovitch, N., Heitman, J. L., Sauer, T. J., Ben-Gal, A. et al., 2014. A review of approaches for evapotranspiration partitioning. Agricultural and Forest Meteorology, 184, 56-70. DOI:http://dx.doi.org/10.1016/j.agrformet.2013.09.003

Lasslop, G., Reichstein, M., Papale, D., Richardson, A. D., Arneth, A., Barr, A., et al., 2010. Separation of net ecosystem exchange into assimilation and respiration using a light response curve approach: critical issues and global evaluation. Biogeosciences, 16, 187–208. doi: 10.1111/j.1365-2486.2009.02041.x

Law, B. E., et al., 2002. Environmental controls over carbon dioxide and water vapor exchange of terrestrial vegetation, Agric. For. Meteorol., 113(1–4), 97–120.

Lawson, T., Vialet-Chabrand, S., 2019. Speedy stomata, photosynthesis and plant water use efficiency. New Phytologist, 221(1), 93-98. DOI:https://doi.org/10.1111/nph.15330

Li, X. et al., 2019. A simple and objective method to partition evapotranspiration into transpiration and evaporation at eddy-covariance sites. Agricultural and Forest Meteorology, 265, 171-182. DOI:https://doi.org/10.1016/j.agrformet.2018.11.017

Li, Z., Qi, F., Wang, Q. J., Song, Y., Li, H., Li, Y., 2016. The influence from the shrinking cryosphere and strengthening evopotranspiration on hydrologic process in a cold basin, Qilian Mountains. Global and Planetary Change, 144, 119–128.

McAusland, L. et al., 2016. Effects of kinetics of light-induced stomatal responses on photosynthesis and water-use efficiency. New Phytol, 211(4), 1209-20. DOI:10.1111/nph.14000

Nelson JA, Pérez-Priego O, Zhou S, et al., 2020. Ecosystem transpiration and evaporation: Insights from three water flux partitioning methods across FLUXNET sites. Glob Change Biol., 00, 1–15.

Papale, D., Reichstein, M., Aubinet, M., Canfora, E., Bernhofer, C., Kutsch, W., Longdoz, B.,

Rambal, S., Valentini, R., Vesala, T., Yakir, D., 2006. Towards a standardized processing of Net Ecosystem Exchange measured with eddy covariance technique: algorithms and uncertainty estimation. Biogeosciences, 3(4), 571-583.

Parazoo, N. C., Bowman, K., Fisher, J. B., Frankenberg, C., Jones, D. B. A., Cescatti, A., Perez-Priego, O., Wohlfahrt, G., Montagnani, L., 2014. Terrestrial gross primary production inferred from satellite fluorescence and vegetation models. Global Change Biology, 20(10), 3103–3121.

Patrick, L. D., Ogle, K., Bell, C. W., Zak, J., Tissue, D., 2009. Physiological responses of two contrasting desert plant species to precipitation variability are differentially regulated by soil moisture and nitrogen dynamics. Global Change Biology, 15(5), 1214–1229.

Perez-Priego, O. et al., 2018. Partitioning Eddy Covariance Water Flux Components Using Physiological and Micrometeorological Approaches. Journal of Geophysical Research: Biogeosciences, 123(10), 3353-3370. DOI:10.1029/2018jg004637

Perez-Ruiz, E. R., Garatuza-Payan, J., Watts, C. J., Rodriguez, J. C., Yepez, E. A., Scott, R. L., 2010. Carbon dioxide and water vapour exchange in a tropical dry forest as influenced by the North American Monsoon System (NAMS). Journal of Arid Environments, 74, 556–563.

Reichstein, M., Falge, E., Baldocchi, D., et al., 2005. On the separation of net ecosystem exchange into assimilation and ecosystem respiration: review and improved algorithm. Global Change Biology, 11(9), 1424-1439.

Scanlon T. M., Kustas, W. P., 2010. Partitioning carbon dioxide and water vapor fluxes using correlation analysis. Agricultural and Forest Meteorology, 2010, 150(1), 89–99.

Schlesinger, W. H., Jasechko, S., 2014. Transpiration in the global water cycle. Agricultural and Forest Meteorology, 189, 115–117.

Scott, R. L., Huxman, T. E., Cable, W. L., Emmerich, W. E., 2006. Partitioning of evapotranspiration and its relation to carbon dioxide exchange in a Chihuahuan Desert shrubland, Hydrol. Process., 20, 3227–3243.

Scott, R. L., Biederman, J. A., Hamerlynck, E. P., Barron-Gafford, G. A., 2015. The carbon balance pivot point of southwestern U.S. semiarid ecosystems: Insights from the 21st century drought, J. Geophys. Res. Biogeosci., 120, 2612–2624.

Scott, R. L., Biederman, J. A., 2017. Partitioning evapotranspiration using long-term carbon dioxide and water vapor fluxes. Geophysical Research Letters, 44, 6833–6840.

Scott, R.L. et al., 2021. Water Availability Impacts on Evapotranspiration Partitioning. Agricultural and Forest Meteorology, 297, 108251.

Smith, W. K., Biederman, J. A., Scott, R. L., Moore, D. J. P., He, M., Kimball, J. S., Yan, D., Hudson, A., Barnes, M. L., MacBean, N., Fox, A. M., Litvak, M. E., 2018. Chlorophyll Fluorescence Better Captures Seasonal and Interannual Gross Primary Productivity Dynamics Across Dryland Ecosystems of Southwestern North America. Geophysical Research Letters, 45, 748–757.

Stillman, S., Ninneman, J., Zeng, X., Franz, T., Scott, R. L., Shuttleworth, W. J., Cummins K., 2014. Summer Soil Moisture Spatiotemporal Variability in Southeastern Arizona. Journal of Hydrometeorology, 15, 1473–1485.

Sun, X., Wilcox, B.P., Zou, C.B., 2019. Evapotranspiration partitioning in dryland ecosystems: A global meta-analysis of in situ studies. Journal of Hydrology, 576, 123-136.

DOI:https://doi.org/10.1016/j.jhydrol.2019.06.022

Sun, Y., Frankenberg, C., Wood, J. D., Schimel, D. S., Jung, M., Guanter, L., Drewry, D. T., Verma, M., Porcar-Castell, A., Griffis, T. J., Gu, L., Magney, T. S., Köhler, P., Evans, B., Yuen, K., 2017. OCO-2 advances photosynthesis observation from space via solar-induced chlorophyll fluorescence. Science, 358, 1–6.

Suni, T., Guenther, A., Hansson, H. C., Kulmala, M., Andreae, M. O., Arneth, A., Artaxo, P., Blyth, E., Brus, M., Ganzeveld, L., Kabat, P. , de. Noblet-Ducoudré, N., Reichstein, M., Reissell, A., Rosenfeld, D., Seneviratne, S., 2015. The significance of land-atmosphere interactions in the Earth system—iLEAPS achievements and perspectives. Anthropocene, 12, 69–84.

Tong, X., Mu, Y., Zhang, J., Meng, P., Li, J., 2019. Water stress controls on carbon flux and water use efficiency in a warm-temperate mixed plantation. Journal of Hydrology. https://doi.org/10.1016/j.jhydrol.2019.02.014

Wang, H., Li, X., Xiao, J., Ma, M., 2021. Evapotranspiration components and water use efficiency from desert to alpine ecosystems in drylands. Agricultural and Forest Meteorology, 298-299, 108283. DOI:https://doi.org/10.1016/j.agrformet.2020.108283

Wang, L., Niu, S., Good, S. P., Soderberg, K., McCabe, M. F., Sherry, R. A., Luo, Y., Zhou, X., Xia, J., Caylor, K. K., 2013. The effect of warming on grassland evapotranspiration partitioning using laser-based isotope monitoring techniques. Geochim. Cosmochim. Acta, 111, 28–38.

Wang, L., Good, S.P., Caylor, K.K., 2014. Global synthesis of vegetation control on evapotranspiration partitioning. Geophysical Research Letters, 41(19), 6753-6757. DOI:10.1002/2014GL061439

Wutzler, T. , Lucasmoffat, A. , Migliavacca, M. , Knauer, Jürgen, Sickel, K., Šigut, L., Menzer, O., & Reichstein, M., 2018. Basic and extensible post-processing of eddy covariance flux data with reddyproc. Biogeosciences, 15, 5015–5030.

Xiao, W., Wei, Z., Wen, X., 2018. Evapotranspiration partitioning at the ecosystem scale using the stable isotope method—A review. Agricultural and Forest Meteorology, 263, 346-361. DOI:https://doi.org/10.1016/j.agrformet.2018.09.005

Yang, X., Tang, J., Mustard, J. F., Lee, J., Rossini, M., Joiner, J., Munger, J. W., Kornfeld, A., Richardson, A. D. 2015. Solar-induced chlorophyll fluorescence that correlates with canopy photosynthesis on diurnal and seasonal scales in a temperate deciduous forest. Geophysical Research Letters, 42, 2977–2987.

Yang, Y. et al., 2016. Contrasting responses of water use efficiency to drought across global terrestrial ecosystems. Scientific Reports, 6, 23284. DOI:10.1038/srep23284

Zhao, W. et al., 2016. Evapotranspiration partitioning, stomatal conductance, and components of the water balance: A special case of a desert ecosystem in China. Journal of Hydrology, 538, 374-386. DOI:http://dx.doi.org/10.1016/j.jhydrol.2016.04.042

Zhou, S., Yu, B., Huang, Y., Wang G., 2014, The effect of vapor pressure deficit on water use efficiency at the subdaily time scale, Geophysical Research Letters, 41, 5005–5013

Zhou, S., Yu, B., Zhang, Y., Huang, Y., Wang, G., 2016. Partitioning evapotranspiration based on the concept of underlying water use efficiency. Water Resources Research, 52, 1160–1175.

Zhou, S., Yu, B., Zhang, Y., Huang, Y., Wang, G., 2018. Water use efficiency and evapotranspiration partitioning for three typical ecosystems in the Heihe River Basin,

northwestern China. Agricultural and Forest Meteorology, 253-254: 261-273. DOI:https://doi.org/10.1016/j.agrformet.2018.02.002